Transport properties and the large anisotropic magnetoresistance of Cu_xNbS_2 single crystals

2009 J. Phys.: Condens. Matter 21 275601

(http://iopscience.iop.org/0953-8984/21/27/275601)

J. Phys.: Condens. Matter **21** (2009) 275601 (7pp) doi:10.1088/0953-8984/21/27/275601

Transport properties and the large anisotropic magnetoresistance of Cu_xNbS_2 single crystals

G Wu[1], T Wu[1], Z Li[2], L Zhao[1], R H Liu[1], H Chen[1], D F Fang[1], J L Luo[2] and X H Chen[1,3]

[1] Hefei National Laboratory for Physical Science at Microscale and Department of Physics, University of Science and Technology of China, Hefei, Anhui 230026, People's Republic of China

[2] Beijing National Laboratory for Condensed Matter Physics, Institute of Physics, Chinese Academy of Science, Beijing 100080, People's Republic of China

E-mail: chenxh@ustc.edu.cn

Received 22 March 2009, in final form 15 May 2009
Published 10 June 2009
Online at stacks.iop.org/JPhysCM/21/275601

Abstract

The transport properties of Cu_xNbS_2 ($x = 0.09$, 0.44 and 0.55) single crystals were systematically studied. The in-plane and out-of-plane resistivities decrease with increasing Cu content, and a transition with hysteresis shows up for the crystals with $x = 0.44$ and 0.55. The thermopower and Hall coefficient of Cu_xNbS_2 show opposite signs, indicating that there are two kinds of carriers in this system. The angular dependences of the in-plane magnetoresistance ($MR_{ab} = (\rho_{ab}(H) - \rho_{ab}(0))/\rho_{ab}(0) \times 100\%$) at different temperatures were also studied. The single crystals with $x = 0.44$ and 0.55 show a strong anisotropic MR_{ab}. For the $x = 0.55$ sample, MR_{ab} reaches 80% with a magnetic field of 14 T applied along the c-axis, while MR_{ab} is less than 5% for the magnetic field applied within the ab-plane. These results can be well understood in the light of the anisotropic Fermi surface in the multiband system.

(Some figures in this article are in colour only in the electronic version)

1. Introduction

The layered transition metal dichalcogenides (TMDs) MX_2 (M = transition metal, X = S, Se, or Te) have been extensively studied due to their two-dimensional structure and physical properties, such as superconductivity and a charge density wave (CDW) transition [1–3]. NbS_2 is one of the layered transition metal dichalcogenides, which have attracted much interest as regards research because of their layered structure with low dimensionality and superconductivity (T_c = 7 K) [2, 3]. NbS_2 is 2H phase; the top sheet and bottom sheet of S atoms stack on each other in a trigonal prismatic manner. The Nb atoms are in the middle of these trigonal prisms [3]. Analogously, many other transition metal dichalcogenides with the same structure, such as 2H-$NbSe_2$, 2H-TaS_2, and 2H-$TaSe_2$, are also superconductors [4, 5]. All these compounds exhibit metallic transport properties. The CDW is another important property of this kind of compound. The coexistence of the superconductivity and CDW, and polymorphic phase transitions, have made layered transition metal dichalcogenides a valuable system, with rich physics, and they are widely studied [1–3].

The interaction between the layers of transition metal dichalcogenides is a weak van der Waals force, so the 3d transition metal atoms can be intercalated into the layers easily [6, 7], like Ag atoms intercalating into 2H-NbS_2. The symmetrical structures of the dichalcogenides may be changed. There are three phases in the Ag_xNbS_2 system with increasing Ag content. For Ag_xNbS_2, when $x \leqslant 0.22$, it is a dilute gas phase, the second-stage phase for $0.22 \leqslant x \leqslant 0.30$, and the first-stage phase for $0.55 \leqslant x \leqslant 0.76$ [8–10]. Bouwmeester *et al* reported the structure, magnetic and electrical properties of $Ag_{0.6}NbS_2$ [9]. In this compound, a phase transition occurs at about 124 K. The transition arises from the Ag atom occupations behaving differently as temperature

[3] Author to whom any correspondence should be addressed.

decreases, changing from disordered to incommensurately ordered [9, 14]. The synthesis and structure of Cu_xNbS_2 have been researched for many years [11–13]. For $Cu_{0.5}NbS_2$, there is a similar phase transition in $Ag_{0.6}NbS_2$ [15–17]. The transition with hysteresis shown in the temperature dependence of the resistance indicates a first-order transition in this system. The Cu^+ ions are disordered at high temperature, while they form a 2×2 superlattice below the transition temperature [15–17].

In the Cu_xNbS_2 or Ag_xNbS_2 system, the Nb atoms are coordinated by chalcogens in trigonal prismatic form. In a trigonal prismatic crystal field, the d_z^2 band is split into two. It can overlap with the top of the s/p valence band [14]. With the intercalation of metal atoms, the increasingly doped electrons start to fill these bands. If the Fermi surface crosses over both the d_z^2 band and the s/p valence band, the system may include two kinds of carriers. The Hall coefficient and thermopower of $Ag_{0.6}NbS_2$ have been studied. It is indicated that the conduction mechanism of two carriers with different mobilities for electrons and holes is responsible for the transport properties [14]. Similar results have also been found for $Cu_{0.5}NbS_2$ [18]. It is well known that there is no magnetoresistance in single-band free electron systems, because the Hall field is balanced by the Lorentz force [19–21]. However, in a multiband conductor, the Hall field cannot be balanced by the Lorentz force, so magnetoresistance might be observed. The anisotropic Fermi surface can lead to large anisotropic magnetoresistance, as observed in MgB_2 [22]. Therefore, a large anisotropic MR is expected in the Cu_xNbS_2 system. In this paper, we report the transport properties of the Cu_xNbS_2 system. The angular dependences of MR_{ab} were measured at different temperatures. It is found that the MR_{ab} anisotropy clearly increases with increasing Cu doping. The $x = 0.55$ sample shows a large anisotropic MR_{ab} with the magnetic field applied along the c-axis and within the in-plane, respectively. These results can be well explained by a multiband electronic structure with different kinds of carriers and an anisotropic Fermi surface in this system.

2. Experiment details

The Cu_xNbS_2 ($x = 0.09$, 0.44 and 0.55) single crystals were grown by the chemical iodine-vapor transport method. Powders of elements Cu (>99.7%), Nb (>99.5%) and S (>99.5%) were mixed and thoroughly ground, then pressed into a pellet. The pellet was sealed under vacuum ($<1.0 \times 10^{-2}$ Pa) in a quartz tube (ϕ13 mm $\times$ 150 mm) with a small quantity of iodine (10 mg/cm^3). The tube was slowly heated to 950 °C in 400 min, and the cold end of the tube was kept at 750 °C for eight days. High quality plate-like Cu_xNbS_2 single crystals were obtained. The single crystals were black and the typical dimension is about $5 \times 5 \times 0.05$ mm^3.

The structure of these crystals was characterized by means of x-ray diffraction (XRD) using a Rigaku D/max-A x-ray diffractometer with Cu Kα radiation ($\lambda = 1.5418$ Å) in the 2θ range of 10°–70° with the step of 0.02° at room temperature. The composition of Cu was determined by x-ray fluorescence spectroscopy (XRF-1800, Shimadzu Inc.). Resistivity measurements were performed using an AC resistance bridge (Linear Research Inc., Model LR700) by the standard four-probe method. The measurement of the magnetoresistance was performed using PPMS systems (Quantum Design). The Hall contact configuration is the standard AC six-probe geometry. To eliminate the offset voltage due to the asymmetric Hall terminals, the magnetic field was scanned from -5 to 5 T. The Hall resistivity shows a linear dependence of the magnetic field. Thermopower measurements were carried out with a home-built apparatus and performed using small and reversible temperature differences of 0.5 K. The two ends of the single crystals were attached to two separated copper heat sinks to generate the temperature gradient across the crystal ab-plane. Two Rh–Fe thermometers were glued to the heat sink (next to the single crystals). Copper leads were adhered to the single crystals, and all of the data were corrected, minus the thermopower of Cu.

3. Results

The XRD patterns at room temperature for the Cu_xNbS_2 single crystals with different $x = 0.09$, 0.44 and 0.55 are shown in figure 1(a). The peaks in the patterns can be indexed with a hexagonal lattice. The c-axis lattice parameter is 13.030 Å for $Cu_{0.55}NbS_2$, 12.998 Å $Cu_{0.44}NbS_2$ and 12.145 Å for $Cu_{0.09}NbS_2$, respectively. All of them are 2H phase and the c-axis parameter becomes larger with increasing Cu content. There is a superstructure for the sample of $Cu_{0.09}NbS_2$ along the c-axis. As shown in the inset of figure 1(a), there are two weak diffraction sub-peaks between the major peaks. This indicates that every three NbS_2 layers, a Cu^+ ion layer is intercalated. It is well known that one unit cell of 2H-NbS_2 includes two trigonal prismatic NbS_6 structures; these two trigonal prisms are opposite to each other. When Cu^+ ions are intercalated into the 2H-NbS_2 structure every three NbS_2 layers, the primary periodicity is broken, and the new unit cell of Cu_xNbS_2 needs six NbS_2 to build its periodic structure. The new unit cell of Cu_xNbS_2 contains six NbS_2 layers along the c-axis and a superstructure is formed. As a result, the superstructure along the c-axis is formed [23, 24]. But for $x = 0.44$ and 0.55 samples, there is no superstructure peak shown in the XRD patterns. The crystal structures of all the samples are shown in figure 1(b).

The temperature dependences of the in-plane (ρ_{ab}) and out-of-plane (ρ_c) resistivities are shown in figures 2(a) and (b) for these Cu_xNbS_2 single crystals. All the samples show a nearly T-linear behavior of ρ_{ab} and ρ_c in most of the temperature range. Metallic character ($d\rho/dT > 0$) is well established. For $x = 0.44$ and 0.55 samples, there are hysteresis loops at about 240 and 265 K, respectively. For the $x = 0.55$ sample, the change in the resistivity is approximately 30% at the transition temperature. This behavior arises from the Cu order–disorder phase transition in this compound. The Cu^+ ions are disordered above the transition temperature, and form a 2×2 superlattice at the transition temperature [15, 16, 25]. Above the transition temperature, the carriers are scattered by the disordered Cu^+

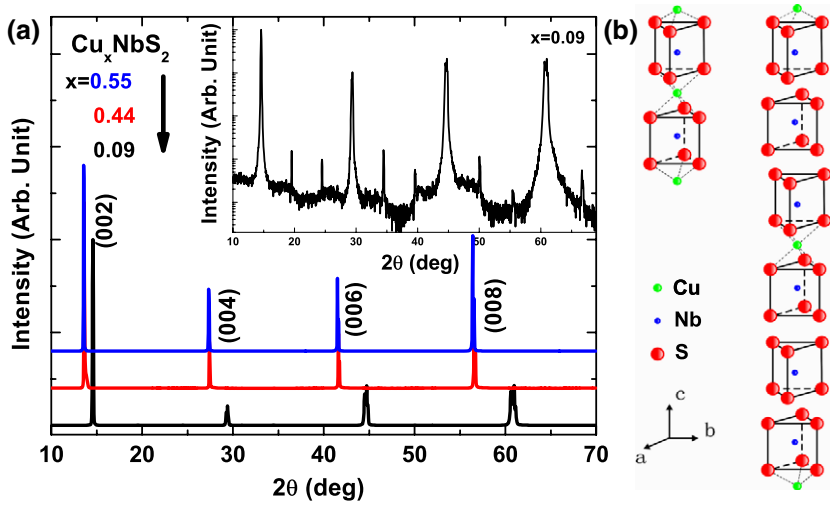

Figure 1. (a) XRD patterns of Cu_xNbS_2 single crystals with different $x = 0.09$, 0.44 and 0.55; only $(00l)$ diffraction peaks show up. The existence of a triple-layered superlattice in the $x = 0.09$ sample is suggested in the upper right inset, where the diffraction intensity is logarithmically rescaled to reveal the construction of the superlattice. (b) Crystal structure of $Cu_{0.44}NbS_2$, $Cu_{0.55}NbS_2$ (left) and $Cu_{0.09}NbS_2$ (right).

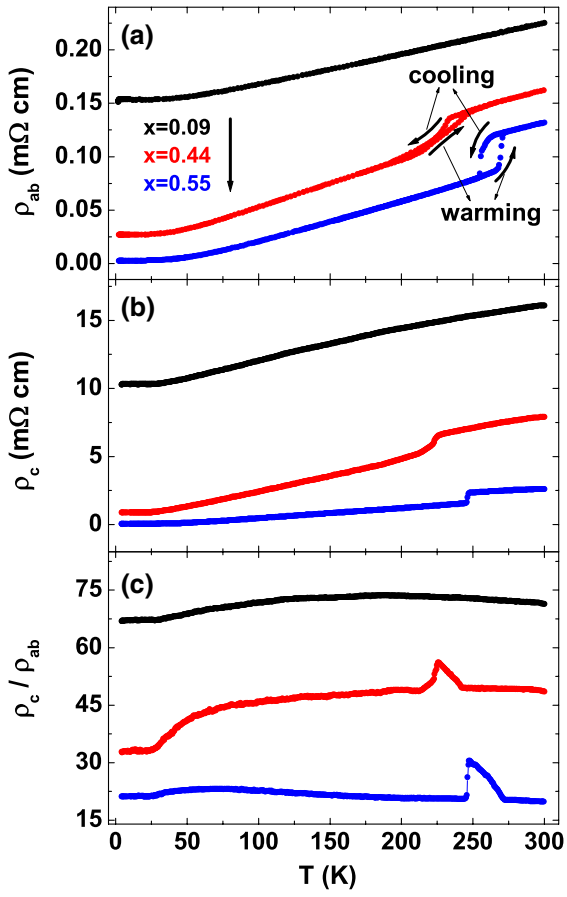

Figure 2. Temperature dependence of (a) the in-plane resistivity (ρ_{ab}) and (b) the out-of-plane resistivity (ρ_c), and (c) the anisotropy ρ_c/ρ_{ab} for Cu_xNbS_2 single crystals with $x = 0.09$, 0.44 and 0.55 measured from 5 to 300 K.

ions. When the superlattice of Cu^+ ions formed with reducing temperature, this kind of scattering is suppressed and the resistivity of the sample decreases [18]. This superlattice is formed by Cu^+ ions ordering in the Cu atom layer, in contrast with the case for other CDW dichalcogenides, in which the superlattice is formed in the TaS_2 layer in TaS_2 [3]. For the $x = 0.55$ sample, the residual in-plane resistivity is as small as 2.7 $\mu\Omega$ cm at about 5 K, and the residual in-plane resistivity ratio ($\rho_{300\ K}/\rho_{5\ K}$) is as large as 50, while it is only 6 for $Cu_{0.44}NbS_2$ and 1.5 for $Cu_{0.09}NbS_2$. As shown in figure 2(b), the out-of-plane resistivity shows similar behavior to the in-plane resistivity for the corresponding samples. Figure 2(c) shows the temperature dependence of the anisotropy ρ_c/ρ_{ab} for the Cu_xNbS_2 system. For 2H-NbS_2, the value of ρ_c/ρ_{ab} is about 2000. With increasing Cu^+ ion content, the anisotropy reduced rapidly. For the $x = 0.09$ sample, the anisotropy is about 70, and it is less than 20 for the $x = 0.55$ sample. The reason is that the 4s orbital of Cu^+ ions can hybridize partly with the $5d_z^2$ orbital of Nb [18]. This suggests that the strong coupling between the Cu^+ ion layers and NbS_2 layers is enhanced by the intercalation of the Cu^+ ions.

Figures 3 and 4 show the temperature dependence of the in-plane thermopower and Hall coefficient for Cu_xNbS_2 with $x = 0.09$, 0.44 and 0.55. In figure 3, the thermopower for all the samples is negative, and it becomes larger with increasing Cu content. A kink is observed in figure 3 at 240 and 265 K for the samples with $x = 0.44$ and 0.55, respectively. The kink observed in the thermopower coincides with the order–disorder phase transition observed in the resistivity, which is shown in figure 2. As shown in figure 4, the Hall coefficient is positive and almost independent of T over the whole temperature range. The Hall coefficient decreases with increasing Cu content. This indicates that the carrier concentration increases with intercalation of Cu^+ ions. As shown in figures 3 and 4, the thermopower and Hall coefficient show opposite signs. This is similar to the behavior of Ag_xNbS_2. Both $Ag_{0.25}NbS_2$ and $Ag_{0.6}NbS_2$ show opposite signs for the thermopower and Hall coefficient over the whole temperature range [26] and 2H-$NbSe_2$, 2H-TaS_2 show similar results at room temperature [27, 28]. It has been explained

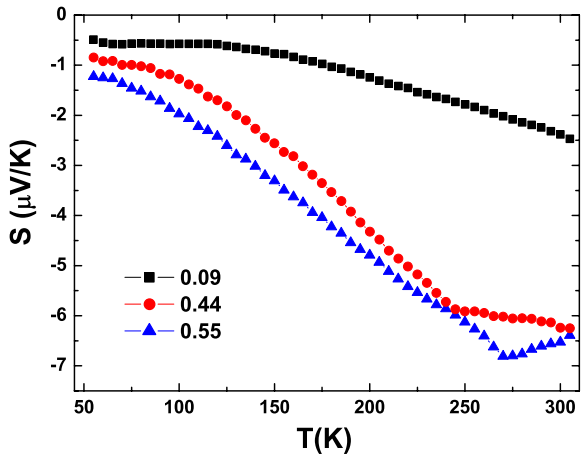

Figure 3. Temperature dependence of the in-plane thermopower for Cu_xNbS_2 single crystals with $x = 0.09$, 0.44 and 0.55.

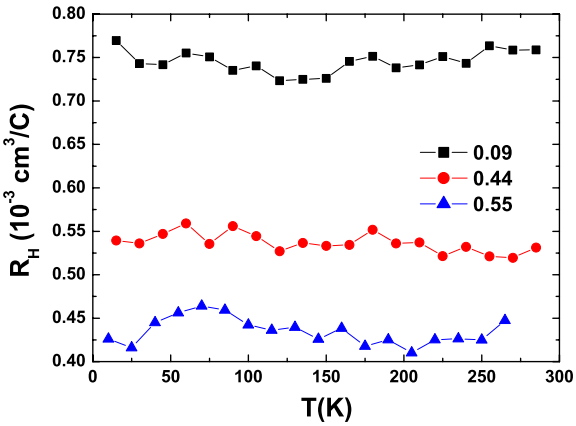

Figure 4. Temperature dependence of the Hall coefficients for Cu_xNbS_2 single crystals with $x = 0.09$, 0.44 and 0.55.

that there exists a two-carrier conduction mechanism in all of these compounds. Both the electron and the hole serve as the carriers, with different mobilities in these compounds [14]. This could be why the large thermopower is observed in the $x = 0.55$ sample with the small Hall coefficient. As shown in figure 4, the Hall coefficient decreases with increasing Cu content. This suggests that the concentration of carriers increases monotonically from $x = 0.09$ to 0.55.

The angular dependence of the in-plane magnetoresistance (AMR_{ab}) is shown in figure 5, at 6, 20 and 50 K. The AMR_{ab} measurements are performed with a rotating H of 10 T. AMR_{ab} shown in figures 5(a)–(c) is obtained by rotating the magnetic field within the ab-plane, while AMR_{ab} shown in figures 5(d)–(f) is obtained by rotating the magnetic field in out-of-plane fashion. At all the temperatures, the magnetoresistance (MR) is very small for the sample with $x = 0.09$. MR_{ab} apparently increases with increasing Cu content. AMR_{ab} is positive and shows a strong angular dependence with a twofold symmetry for the samples with $x = 0.44$ and 0.55. AMR_{ab} shows a strong anisotropy with decreasing temperature. In the two kinds of rotations, when $H \perp I$, MR_{ab} reaches a maximum,

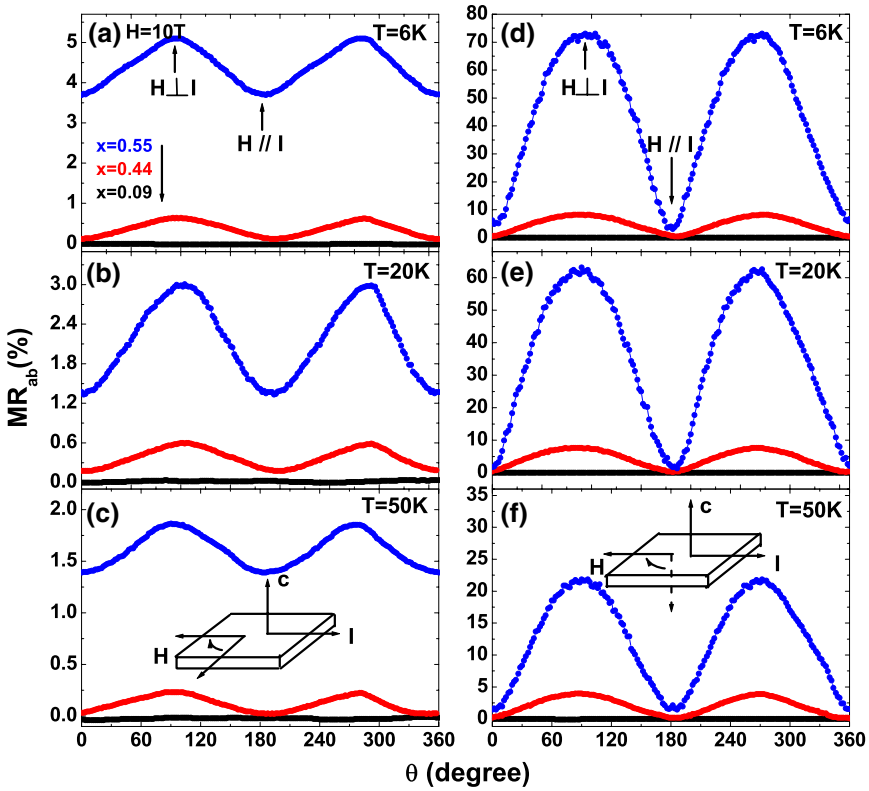

Figure 5. The in-plane MR_{ab} as a function of angle for Cu_xNbS_2 single crystals at different temperatures (6, 20 and 50 K) with the field $H = 10$ T. θ is the angle between the magnetic field H and current I directions, and is changed by rotating H. The results shown in (a)–(c) are obtained with rotating H in the ab-plane; the results shown in (d)–(f) are obtained with rotating H in the plane consisting of the current and the c-axis.

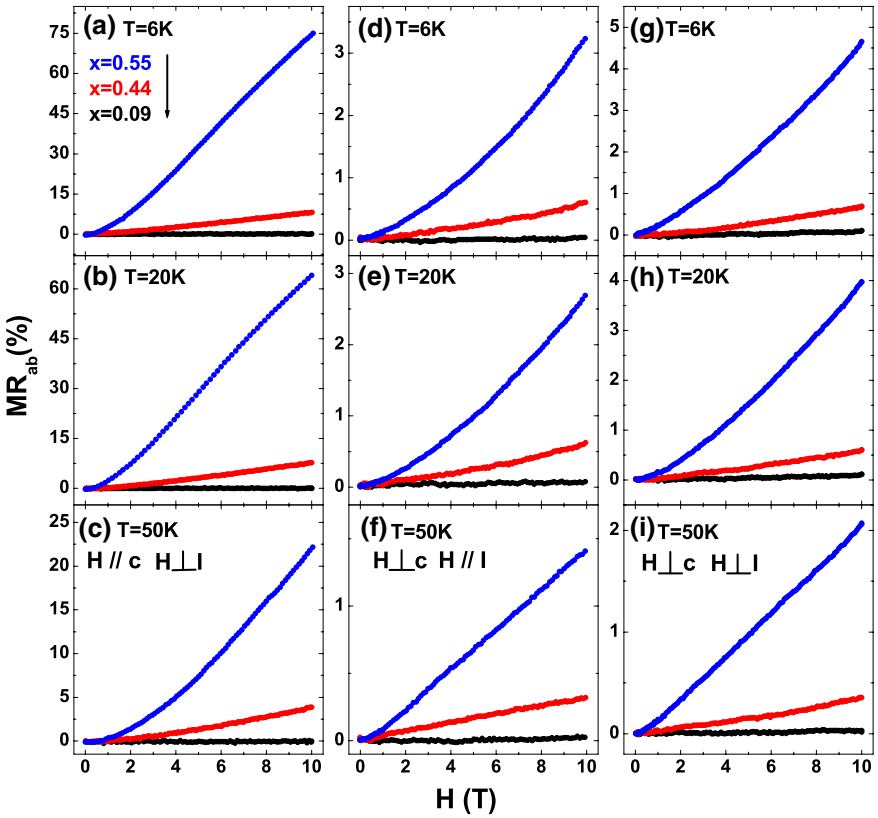

Figure 6. The in-plane isothermal MR_{ab} as a function of H for $x = 0.09$, 0.44 and 0.55 Cu_xNbS_2 single crystals at 6, 20 and 50 K under H with different directions. The relative directions of the magnetic field H, current I and c-axis are shown in the figure; in (a)–(c): $H \parallel c$ and $H \perp I$; in (d)–(f): $H \perp c$ and $H \parallel I$; in (g)–(i): $H \perp c$ and $H \perp I$.

while when $H \parallel I$, MR_{ab} is minimum. For the $x = 0.55$ sample, MR_{ab} is nearly 75% with $H \parallel c$ at 6 K, while it is only about 5% with H within the ab-plane. A similar behavior is observed for the sample $Cu_{0.44}NbS_2$.

The isothermal MR with H along three different directions is shown in figure 6. For the $x = 0.09$ sample, hardly any MR_{ab} can be observed for H along the different directions. For $x = 0.44$ and 0.55 samples, the largest MR_{ab} at the same temperature is observed with $H \parallel c$. It is well known that the MR behavior should follow Kohler's rule if there is only one relaxation time existing in a solid [19]. The MR must be a function of $H/\rho(0)$, and the results at different temperatures can superpose on each other in the plot of MR versus $H/\rho(0)$. $\rho(0)$ is the resistivity at a fixed temperature without a magnetic field. MR_{ab} for $Cu_{0.55}NbS_2$ single crystal as a function of the $H/\rho_{ab}(0)$ is shown in figure 7. For the $x = 0.55$ sample, the MR behavior does not follow Kohler's rule in different directions. This indicates that Cu_xNbS_2 is a multiband system.

4. Discussion

The Hall coefficient only depends on the carrier concentration. The thermopower can be expressed as equation (1).

$$S = \frac{\pi^2 k_B^2 T}{3e}\left(\frac{\mathrm{d}\ln(\mu_0 N)}{\mathrm{d}E}\right) \tag{1}$$

where $\mu_0 = eL^2/\tau_0 k_B T$ (L^2/τ_0 corresponds to the diffusion constant for a random walk of carriers), N is the density of states at the Fermi surface [29]. For a single-band system, the thermopower and Hall coefficient $R_H = \frac{1}{ne}$ must have the same signs. But in the Cu_xNbS_2 system, they have opposite signs as shown in figures 3 and 4. This result cannot be understood in a single-band model. If there are two bands around the Fermi surface, the thermopower and Hall coefficient can be expressed by equations (2) and (3) [30–32].

$$S = \frac{\pi^2 k_B^2 T}{3e}\left(\frac{\mathrm{d}\ln(\mu_0 N_e)}{\mathrm{d}E} + \frac{\mathrm{d}\ln(\mu_0 N_p)}{\mathrm{d}E}\right) \tag{2}$$

$$R_H = \frac{n_p\mu_p^2 - n_e\mu_e^2}{e(n_p\mu_p + n_e\mu_e)^2} \tag{3}$$

where the N_e and N_p in equation (2) are the density of states for electrons and holes at the Fermi surface, respectively, and in equation (3) n and μ are the concentration and mobility of the carriers. The sign of the thermopower is decided by $\frac{\mathrm{d}\ln(\mu_0 N_e)}{\mathrm{d}E} + \frac{\mathrm{d}\ln(\mu_0 N_p)}{\mathrm{d}E}$, and the Hall coefficient is proportional to $\frac{n_p\mu_p^2 - n_e\mu_e^2}{n_p\mu_p^2 + n_e\mu_e^2}$. In this situation, the signs of the Hall coefficient and thermopower can be opposite. This suggests that the Cu_xNbS_2 is a multiband conductor with two kinds of carriers as in the Ag_xNbS_2 system [14].

An unusually large MR_{ab} is observed in the $Cu_{0.55}NbS_2$ sample as shown in figures 5 and 6. This kind of large

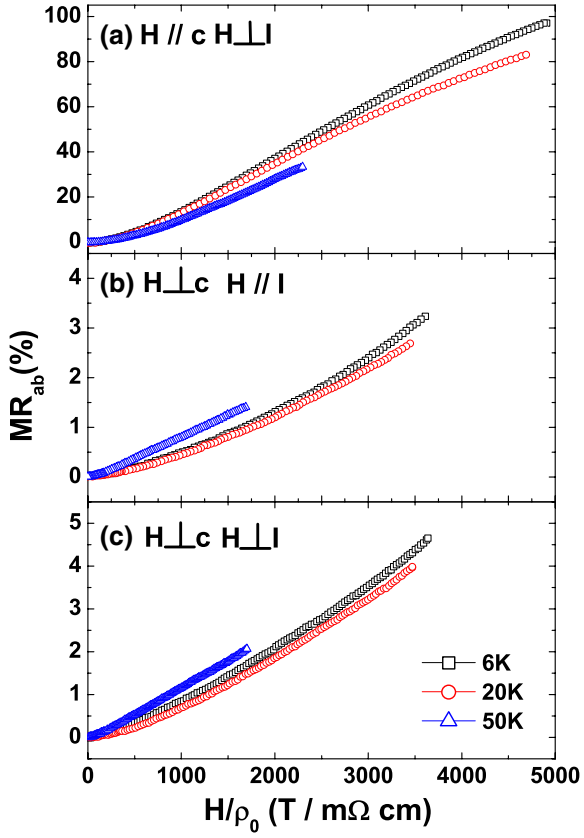

Figure 7. Kohler plot for $Cu_{0.55}NbS_2$ at 6, 20 and 50 K in different relative directions among the magnetic field H, current I and c-axis. Their relative directions are shown in the figure; in (a): $H \parallel c$ and $H \perp I$; in (b): $H \perp c$ and $H \parallel I$; in (c): $H \perp c$ and $H \perp I$.

magnetoresistance cannot be understood through a single-band mechanism of conduction. In a single-band system, the Hall field exactly balances the Lorentz force, and there will be no magnetoresistance [19–21]. Such large MR_{ab} can be explained by multiband electronic structure with different kinds of carriers. In the Cu_xNbS_2 system, when the Cu^+ ions are intercalated into the layers, the d_z^2 band may overlap with the top of the s/p valence band [14]. If the Fermi surface crosses over both the d_z^2 band and the s/p valence band, the system will include two kinds of carriers: electrons and holes. They have opposite signs, different relaxation times τ, and different effective masses m^* and cyclotron frequencies ω_c. For the low field limit ($\omega_c\tau \ll 1$), the magnetoresistance $\Delta\rho/\rho_0$ can be expressed by equation (4) [19, 21].

$$\frac{\Delta\rho}{\rho_0} \simeq \frac{1}{2}\frac{\Sigma_i \Sigma_{j\neq i}\sigma_i\sigma_j(\omega_{ci}\tau_i - \omega_{cj}\tau_j)^2}{(\Sigma_i\sigma_i)}. \quad (4)$$

For a hole-like band, $\omega_c > 0$, while for an electron band, $\omega_c < 0$. Here, σ_i and σ_j are weighting factors. The value of $\Delta\rho/\rho_0$ is close to $(\omega_{ci}\tau_i - \omega_{cj}\tau_j)^2$. Because of the opposite signs of ω_{ci} and ω_{cj} in the Cu_xNbS_2 system, the value of $(\omega_{ci}\tau_i - \omega_{cj}\tau_j)^2$ tends to be larger than that of the same-signed ω_{ci} and ω_{cj}; therefore a large magnetoresistance is expected in Cu_xNbS_2. For the $x = 0.55$ sample, MR_{ab} is as large as 75% when the high field is applied along the c-axis as shown in figure 6.

But there is another puzzle: why MR_{ab} with $H \parallel c$ for the $x = 0.55$ sample is 75% at 6 K, while it is only 7% for the $x = 0.44$ sample. In the free electron multiband picture, if $\omega_c\tau \geqslant 1$, the Lorentz force will lead to a large contribution to magnetoresistance when the magnetic field is perpendicular to the electric current direction. If $\omega_c\tau \ll 1$ or the magnetic field is parallel to the electric current direction, this contribution will disappear [20]. This criterion has also been used for MgB_2 thin films [22]. In order to explain this result, we estimated the average value of $\omega_c\tau$ for $x = 0.09$, 0.44 and 0.55 samples at 6 K from the Hall coefficient and residual resistivity in this work. $\omega_c\tau$ is ~0.05 for the $x = 0.09$ sample, ~0.2 for $x = 0.44$ and ~1.5 for $x = 0.55$. This suggests that the Lorentz force leads to a larger contribution to the magnetoresistance for the $x = 0.55$ sample, while this kind of contribution is negligible for the $x = 0.09$ sample. It becomes easy to understand why the magnetoresistance of the $x = 0.55$ sample for $H \parallel c$ is much larger than those for other compositions.

The strong anisotropic magnetoresistance is also interesting in this system. ARPES results show an anisotropic Fermi surface in NbS_2 [33]. With the analogous structure, an anisotropic Fermi surface should be expected in Cu doped NbS_2. Such strong anisotropy in MR_{ab} should be closely related to the anisotropic Fermi surface in the two-carrier multiband Cu_xNbS_2 system. When the direction of the applied field changes, the orbital plane of the electron intercepts the Fermi surface at different angles, and ω_{ci} should also be changed. When $H \perp ab$, ω_{ci} is large for the orbit in this situation. According to equation (4), the value of $(\omega_{ci}\tau_i - \omega_{cj}\tau_j)^2$ leads to a larger magnetoresistance with two kinds of carriers. When $H \parallel ab$, ω_{ci} is small or partly reduced, just like the case for the MgB_2 system [22], so the magnetoresistance is small. In this picture, this large anisotropy of the magnetoresistance can be well understood. In the Cu_xNbS_2 system, the large magnetoresistance arises from the multiband electronic structure, and the anisotropic Fermi surface leads to strong anisotropy in the magnetoresistance.

5. Conclusion

In summary, we have grown high quality Cu_xNbS_2 single crystals with $x = 0.09$, 0.44 and 0.55. The anisotropic resistivity, thermoelectric power, Hall coefficients and AMR_{ab} are systematically studied. In Cu_xNbS_2, a large magnetoresistance and its strong anisotropy are observed. In the multiband conductor, there are two kinds of carriers, and an anisotropic Fermi surface exists in Cu_xNbS_2. These lead to large magnetoresistance and strong anisotropic magnetoresistance. Similar phenomena have been reported for the clean MgB_2 system with a multiband [22]. In this picture, the large magnetoresistance and its strong anisotropy in the Cu_xNbS_2 system can be well understood.

Acknowledgments

This work was supported by a grant from the Natural Science Foundation of China and by the Ministry of Science

and Technology of China (973 project No. 2006CB601001) and by the National Basic Research Program of China (2006CB922005).

References

[1] Wilson J A and Yoffe A D 1969 *Adv. Phys.* **18** 193
[2] Friend R H and Yoffe A D 1987 *Adv. Phys.* **36** 1
[3] Wilson J A, Di Salvo F J and Mahajan S 1975 *Adv. Phys.* **24** 117
[4] Di Salvo F J, Hull G W Jr, Schwartz L H, Voorhoeve J M and Waszczak J V 1973 *J. Chem. Phys.* **59** 1922
[5] Naito M and Tanaka S 1982 *J. Phys. Soc. Japan* **51** 219
[6] Whittingham M S 1978 *Prog. Solid State Chem.* **12** 41
[7] Trichet L, Rouxel J and Pouchard M M 1975 *J. Solid State Chem.* **14** 283
[8] Van Der Lee A, Wiegers G A, Haange R J and de Boer J L 1990 *Acta Crystallogr.* C **46** 976
[9] Bouwmeester H J M 1985 *Solid State Ion.* **16** 163
[10] Van Der Lee A, van Smaalen S, Wiegers G A and de Boer J L 1991 *Phys. Rev.* B **43** 9420
[11] Koerts K 1963 *Acta Crystallogr.* **16** 432
[12] Nitsche R and Wild P 1968 *J. Cryst. Growth* **34** 153
[13] Boswell F W, Prodan A and Corbett J M 1976 *Phys. Status Solidi* a **35** 591
[14] Bouwmeester H J M, Van Der Lee A, van Smaalen S and Wiegers G A 1991 *Phys. Rev.* B **43** 9431
[15] de Ridder R, van Tendeloo G, van Landuyt J, van Dyck D and Amelincks S 1976 *Phys. Status Solidi* a **37** 591
[16] de Ridder R, van Tendeloo G, van Landuyt J, van Dyck D and Amelincks S 1976 *Phys. Status Solidi* a **38** 185
[17] de Ridder R, van Tendeloo G, van Landuyt J, van Dyck D and Amelincks S 1977 *Phys. Status Solidi* a **39** 383
[18] Pfalzgraf B W, Spreckels H, Paulus W and Schöllhorn R 1987 *J. Phys. F: Met. Phys.* **17** 875
[19] Ziman J M 2001 *Electrons and Phonons, Classics Series* (New York: Oxford University Press)
[20] Kittel C 1993 *Quantum Theory of Solids* (New York: Wiley)
[21] Callaway J 1976 *Quantum Theory of the Solid State* (New York: Academic)
[22] Li Qi, Liu B T, Hu Y F, Chen J, Gao H, Shan L, Wen H H, Pogrebnyakov A V, Redwing J M and Xi X X 2006 *Phys. Rev. Lett.* **96** 167003
[23] Scholz G A, Frindt R F and Curzon A E 1982 *Phys. Status Solidi* a **71** 531
[24] Scholz G A, Frindt R F and Curzon A E 1982 *Phys. Status Solidi* a **72** 375
[25] Boebinger C S, Wakefield N I F, Marseglia E A, Friend R H and Tatlock G J 1983 *Physica* B+C **117/118B** 608
[26] van Maaren M H and Harland H B 1969 *Phys. Lett.* A **29** 571
[27] Lee H N S, Garcia M, McKinzie H and Wold H 1970 *J. Solid State Chem.* **1** 190
[28] Thompson A H, Gamble F R and Koehler R F Jr 1972 *Phys. Rev.* B **5** 2811
[29] Cutler M and Mott N F 1969 *Phys. Rev.* **181** 1336
[30] Hurd C M 1972 *The Hall Effect in Metals and Alloys* (New York: Plenum)
[31] Ziman J M 1964 *Principles of the Theory of Solids* (Cambridge: Cambridge University Press)
[32] Sondheimer E H 1948 *Proc. R. Soc.* A **193** 484
[33] Battaglia C, Cercellier H, Despont L, Monney C, Prester M, Berger H, Forro L, Garnier M G and Aebi P 2007 *Eur. Phys. J.* B **57** 385